Grid Synchronization during Non-Ideal Grid Conditions Based on Double Integration Method

Kamran Hafeez *‡, Mohannad Jabbar Mnati**, Alex Van Den Bossche ***

* Electrical and Computer Engineering department, COMSATS University, Islamabad 444000, Pakistan

** Department of Electrical Technology, Institute of Technology Baghdad, Middle Technical University, Al- Za'franiya, 10074 Baghdad, Iraq

*** Laboratory of Electrical Energy-EELAB, Faculty of Engineering and Architecture, Ghent University 9000, Belgium

(voltagehigh@hotmail.com , Mohannad.mnati@mtu.edu.iq , Alex.VandenBossche@ugent.be)

‡ Corresponding Author; Kamran Hafeez, 444000, Tel: +92 314 90 37950,

voltagehigh@hotmail.com

Received: 26.09.2023 Accepted:10.11.2023

Abstract- Modular multilevel converter (MMC) has numerous advantages already discussed in the literature. Grid voltage synchronization is a critical component of grid-connected power converters. Synchronous reference frame (SRF)-PLL traditionally synchronizes MMC voltage to the grid. However, non-ideal grid circumstances induce phase angle inaccuracies since phase angle is obtained by integrating grid frequency. The three-phase dual integration method (DIM) is used in the grid synchronization of a three-phase MMC inverter in this study. It integrates grid phase voltage twice to generate reference signals for the MMC grid side converter. Furthermore, it enables a smooth start during balanced and non-ideal grid conditions a) voltage unbalance; and b) frequency unbalance, as the generated signal remains in phase with the current. The proposed process reduces THD to almost less than (< 0.09%). The simulation results demonstrate the suggested method's efficacy in grid synchronization.

Keywords SRF-PLL, HVDC, Grid synchronization, Transmission system, Power converter.

1. Introduction

The most effective technology for high-voltage DC transmission networks is the modular multilevel converter (MMC) [1]. Numerous benefits include its modular design, decreased power supply in each module, lower harmonic content, and staircase output voltage [2]. An effective grid synchronization technique is necessary for the integration of renewable energy with HVDC systems [3]. A synchronously rotating d-q reference frame (SRF-d-q) or a fixed reference frame (SRF-d-q) is used in building GSPC (grid-side power converter). (PCC) Point of common coupling in SRF-d-q, phase angle of grid voltage, the frequency are retrieved by monitoring three-phase current/voltages and converting them into two-phase d-q current components [4-5]. In addition to the closed loop, the open-loop, ZCD (zero crossing detection), and artful intelligence (AI) [7] are further grid synchronization systems.

Three-phase grid voltages are converted from SRF-PLL to d-q rotating frame as shown in Figure 1 Park's transformation [12] is used. Eq. (1) depicts the d-axis and q-axis components under balanced grid conditions.

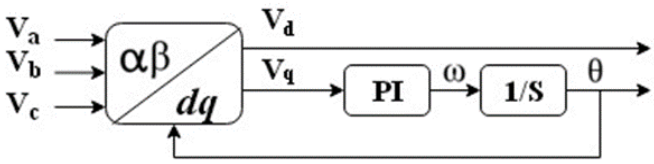

Fig. 1. SRF-PLL Basic structure.

$$\begin{bmatrix} V_d \\ V_q \end{bmatrix} = \begin{bmatrix} \cos\theta & \sin\theta \\ -\sin\theta & -\cos\theta \end{bmatrix} \begin{bmatrix} V\cos\theta' \\ V\sin\theta' \end{bmatrix} = \begin{bmatrix} V\cos(\theta' - \theta) \\ V\sin(\theta' - \theta) \end{bmatrix} \quad (1)$$

Where: V, θ' represent the phase and capacity for input voltage signal, θ is the PLL output, V_d, and V_q is the d and q axis components.

The voltage signal's amplitude is shown on the d-axis, while the phase angle data is shown on the q-axis. However, in non-ideal grid settings, phase angle tracking in SRF-PLL deviates; a) DC-offsets, b) imbalance voltages, and c) harmonics [13-15]. DC-offset is caused by sampling mistakes in A/D conversion and the insertion of DC components [16-

19]. Many solutions to the problem of DC offsets in a PLL have been offered in the literature. In [20]. A bandpass filter is used; however, it creates a phase shift as the frequency changes. In [21] fundamental components are extracted at the input of a PLL, However, exact DC component computation is essential. SOGI-PLL is proposed for the elimination of DC components in a single-phase system [22-26]. In order to achieve grid synchronization in less-than-ideal grid conditions, discretely coupled synchronous reference frame (DDSRF-PLL) is eligible, however, the problem of the DC offset remains unsolved [27]. proposes employing analog circuits single phase inverter grid synchronization by double integration. This paper suggests a three-phase grid-connected solar PV inverter with double integration [28] that only considered steady-state situations.

The key contribution of this paper is to implement grid coincidence in Three phase MMC converter using a Three-phase DIM. The DIM methods already proposed in [27-28] have different approaches. The current amplitude is corrected using MPPT in a single-phase Inverter based on analog circuit, here in this work gain values of controllers are adjusted to adjust the amplitude of current in a digital circuit. Unlike [28] that synchronize Inverter current with a grid voltage, this research work also considers dynamic or non-ideal conditions in a grid. Since the generated signal remains in phase with the current, the DIM method works well during dynamic conditions.

Without paying attention to phase angle or frequency, reference currents are generated by the three-phase DIM by using phase voltage or line-to-line obtained from the grid, as shown in Eq. (2) [29].

$$i_{\mathrm{ref}} = \iint \mathrm{V_p} \qquad (2)$$

Where: $\boldsymbol{i_{ref}}$ are the current references, while V_p denotes grid phase voltage.

Eq. (1) is used to represent the DIM block diagram in Figure 2. The outputs of the first and second integrals, Y_a and Y_b, respectively, correspond to the input voltage of a signal. Two PI controllers are set in the feedback path to minimize the DC offset in each integral part.

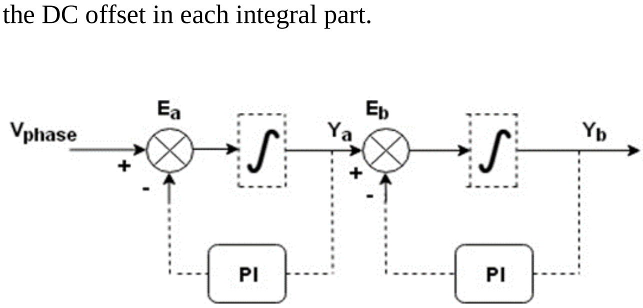

Fig. 2. Block diagram of DIM.

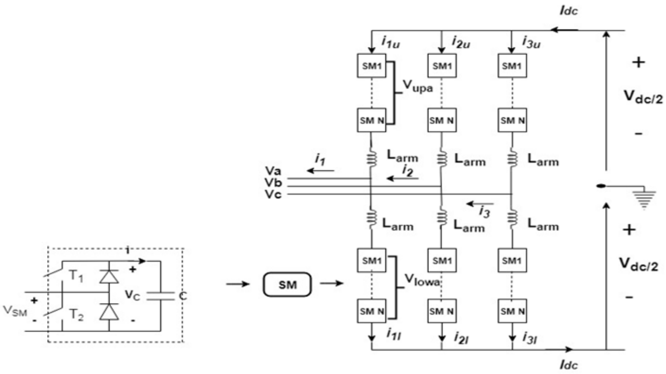

Fig. 3. Three-phase MMC structure.

This paper is systematic as Section 2 describes the Three-phase MMC structure, Section 3 presents the digital implementation of Three-phase DIM circuit l, Section 4 presents the simulation results in a Three-phase grid connection using PSCAD, Section 5 concludes with a comparison with alternative grid synchronization strategies.

2. MMC Modelling

A Three-phase MMC structure consists of two identical arms in each phase with n the chain is connected to sub-modules (SMs) and an inductor as shown in Figure 3. Each SM has a single capacitor and the switches are two Linked series (T1, T2). The control system determines whether the SM output voltage (V_{sm}) is equal to the capacitor voltage (T1 on state) or zero (T2 off state) [30-31]. It can be modelled in EMT-type programs by approximating the behaviour of lumped passive elements based on numerical integration methods [32]. The full specifics of various modelling methodologies are detailed in [33]. In this paper an arm equivalent model of MMC is developed based on the fundamental switching frequency and switching patterns of IGTBT are neglected as already discussed [34].

3. MMC Three-Phase Double Integration Method

The block design in Figure 2 is used to create a three-phase DIM using PSCAD. Double integrators 180° rotate the phase voltage signal to coincide with the grid voltages. as shown in Eqs. (3-5), the Three-phase grid voltages are input into the DIM model.

$$\mathrm{V_{p1}(t)} = \sqrt{2}\boldsymbol{V}sin(\omega_o t) \qquad (3)$$

$$\mathrm{V_{p2}(t)} = \sqrt{2}\boldsymbol{V}\sin\left(\omega_o t - \frac{2\pi}{3}\right) \qquad (4)$$

$$\mathrm{V_{p3}(t)} = \sqrt{2}\mathbf{V}\sin\left(\omega_o \mathrm{t} + \frac{2\pi}{3}\right) \qquad (5)$$

Where: V represents RMS value for the phase voltage, V_m=2 V represents a peak voltage, the (o) represents the grid frequency.

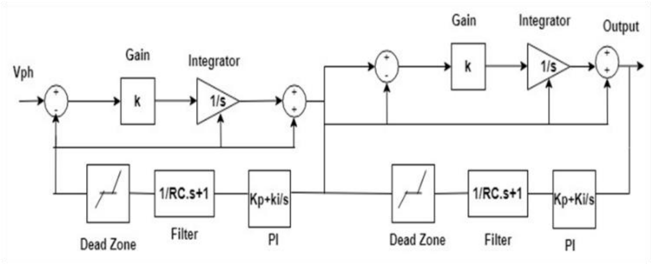

Fig. 4. Three-phase grid synchronization using DIM.

In Eq. (6), the closed-loop transfer function can be derived;

$$\frac{Output}{Input} = \frac{G}{1 + GH} = \frac{s(s+1)}{s(\,s^2 + s + k_p + k_{i/s})} \qquad (6)$$

Where: $H(s) = (1/s + 1) * (k_p + k_i/s),\ \ ),\ \ G(s) = 1/s$, feedback and forward flow for the closed-loop system are shown. Signal input may be written as in Eq. (7);

$$b(t) = C_m \sin(\omega_o t) \qquad (7)$$

Where: C_m and ω_o is the input signal's amplitude and frequency. The outputs of the double integration can calculate as in Eq. (8);

$$z(t) = C_n \sin(\omega t + \varphi) \qquad (8)$$

Where: φ and C_n, ω, are the capacity, The output signal's frequency, and phase angle.

Bode plots, as illustrated in Figure 5, may be used to derive the frequency response characteristics of double integrals. Since the output of double integrals creates a phase shift of -180°, the Voltage signal produced is synchronized to the grid voltages after being multiplied by k=-1.

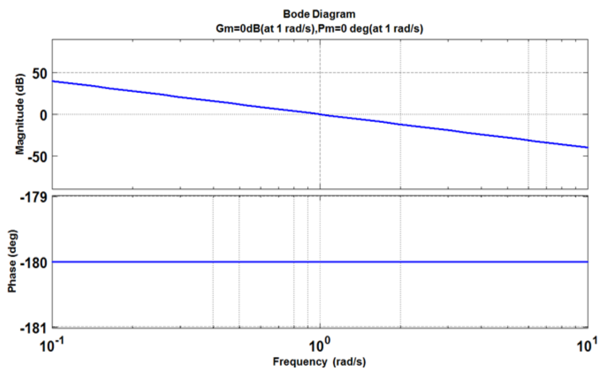

Fig. 5. Double Integrals' frequency response.

A pure integrator's output signal will have issues with DC offset and drift. [35]. Phase errors are introduced for the removal of DC offset using a high pass filter [36].

Applying 2nd order generalized integrator into SRF-PLL during non-ideal conditions will affect its settling time and speed [37]. Proportional integral (PI) based compensator ***k_p+ki/s*** is designed in a non-linear feedback path to perform two functions a) Integrator clamping and b) reject DC offset at each integrator. The integrating constant can be reset if the maximum or minimal integral is reached and also has no DC component.

The effect is that it is clamped in the first half period and the next periods, the residual DC is removed. In a steady state, there will be no interaction of the feedback, as then the phase is exactly 180° even if the frequency changes. A leading phase shift occurs as a result of linear lagging feedback, which grows as the feedback gain rises. As seen in Figure 6, any time this repair is necessary, it can be resolved by adding a dead zone after the low pass filter. This dead zone will make it a nonlinear feedback system and only acts when a DC offset occurs. The low pass filter RC value is selected as 0.0031 to cut off frequency around 50 Hz. The frequency response of PI controllers is shown in Figure 7. The k_p and ki values are selected as 1.32 and 6.07 respectively to give a phase margin of 50 degrees to make the system stable. As long as non-linear feedback is active, DIM recovers naturally from transients.

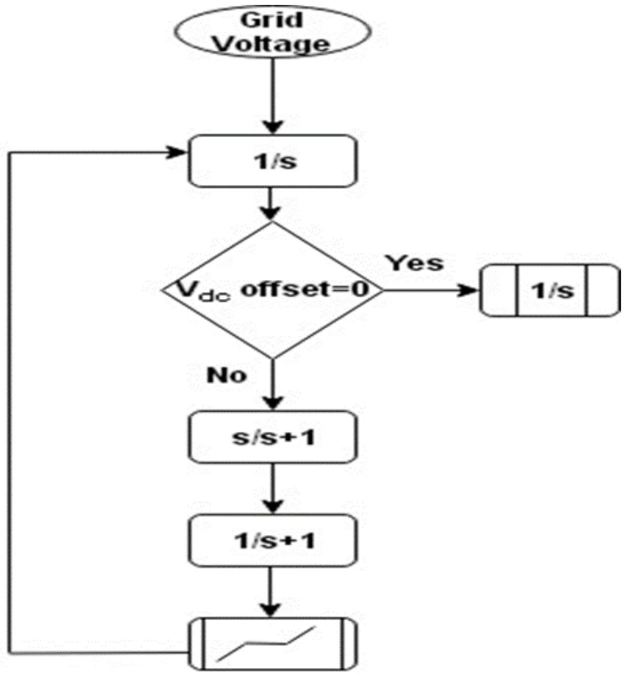

Fig. 6. Integration constant removal.

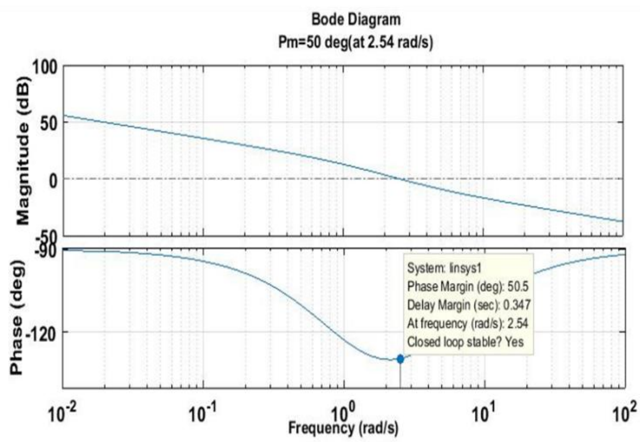

Fig. 7. Frequency response of PI controllers.

4. Simulation Results Three-Phase DIM Grid Connected

The three-phase MMC in inverter mode is linked to the power AC grid (L_{ac}) with an AC filter (L_1, R_1) as shown in Figure 8. In an HVDC system, the current source (I_1) is used to represent the DC grid. The frequency and phase of Three-phase voltages are important for synchronization and control of grid connected MMC [38].

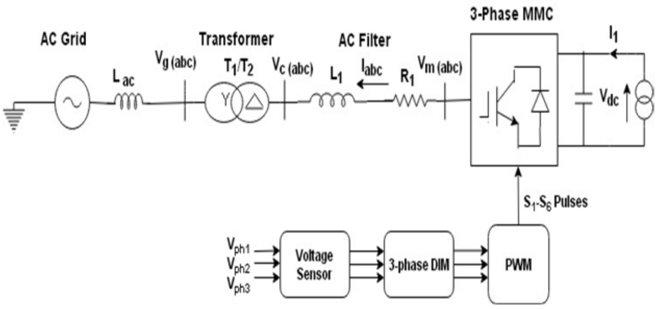

Fig. 8. Three-phase MMC inverter.

A direct modulation method based on an open loop modulator is implemented in this paper to calculate insertion indices for each arm in a three-phase MMC converter. The inserted arm voltages are $Vc=n_u\ V_u^{\Sigma}$, where n_u indicates insertion indices and V_u^{Σ} is the total voltage of the capacitors in each arm [39]. A separate controller is used to suppress the circulating current [40]. As seen in Eqs. (9-10) the reference signal provides sinusoidally output current and voltage on the AC side of MMC;

$$V_s = \boldsymbol{V_s} cos\omega_o t \quad (9)$$

$$I_s = \boldsymbol{I_s} cos\omega_o t \quad (10)$$

Where: I_s and V_s are the maximum AC side current and voltage parameters of the MMC converter ω_o are the fundamental frequency in radians per second.

The MMC grid-connected inverter shown in Figure 8 is tested under the following nonideal grid conditions:

4.1. Three-phase voltage unbalance;

$$V_{p1} = 0.9V_m \sin(\omega t) \quad (11)$$

$$V_{p2} = 0.8\, V_m \sin(\omega t - \frac{2\pi}{3}) \quad (12)$$

$$V_{p2} = 1.2V_m \sin(\omega t + 2\pi/3) \quad (13)$$

4.2. Three-phase frequency unbalance;

$$V_{p1} = V_m \sin(2 * pi * 0.95f * t) \quad (14)$$

$$V_{p2} = V_m \sin\left(2 * pi * 0.97f * t - \frac{2\pi}{3}\right) \quad (15)$$

$$V_{p3} = V_m \sin\left(2 * pi * 1.03f * t + \frac{\pi}{3}\right) \quad (16)$$

Based on Eqs. (3-5), Figure 9 (a-c) depicts the results of emulation for the Three-phase DIM utilized in grid synchronization of the MMC Inverter for 50 Hz Grid frequency. Figure 9 (a) depicts three-phase balanced AC network voltages. Figure 9 (b) shows the output of the DIM synchronizing grid voltage input Black phase at t=0.005s Figure 9 (c) shows the output of the DIM synchronizing grid voltage input light blue phase at t=0.005s. DC–offset is eliminated on each integrator. Figure 9 (d) shows the output of DIM synchronizing grid voltage input blue phase at t=0.005s.

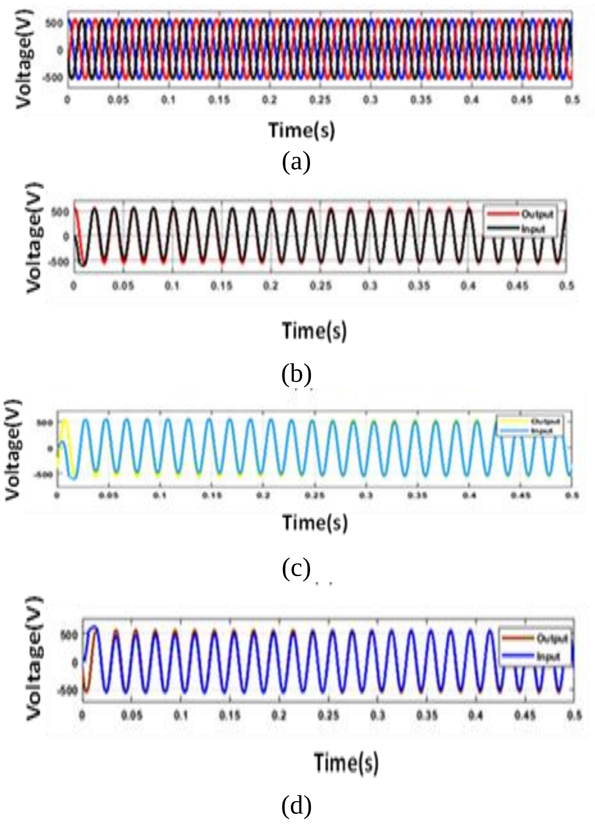

Fig. 9. DIM results for three phases (50 Hz): a) maintain grid voltage balance, b) Output of DIM black phase, c) Output DIM light blue phase, and d) Output DIM blue phase.

Figure 10 shows the results of a three-phase DIM simulation carried out during non-ideal grid conditions in an MMC inverter based on Eqs. (11-13). Figure 10 (a) shows Three-phase unbalanced voltages. Figure (b) shows the output of DIM synchronizing grid voltage input red phase at t=0.005s Figure 10 (c) shows the output of DIM synchronizing grid voltage input light blue phase at t=0.005s. DC-offset is eliminated on each integrator. Figure 10 (d) shows the output of DIM synchronizing grid voltage input blue phase at t=0.005s.

Figure.11 shows the simulation results of Three-phase DIM implemented during nonideal grid conditions based on Eqs. (14-16). Figure 11 (a) shows the Three-phase unbalance frequency voltages. Figure 11 (b) shows the output of the DIM synchronizing grid voltage input Blue phase at t=0.005s Figure 11 (c) shows the output of the DIM synchronizing grid voltage input black phase at t=0.005s. Figure 11 (d) shows the output of DIM synchronizing unbalanced frequency grid voltage input yellow phase at t=0.005s.

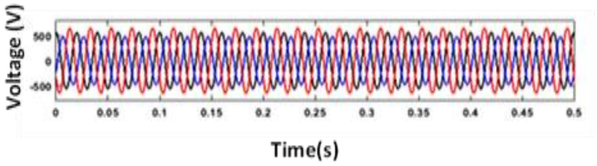

(a)

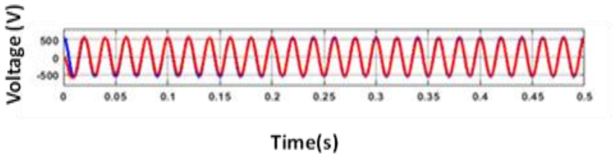

(b)

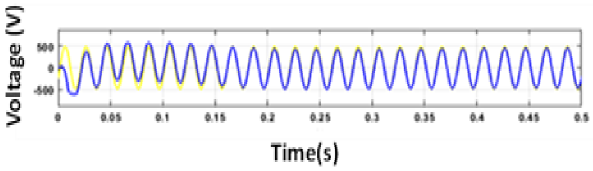

(c)

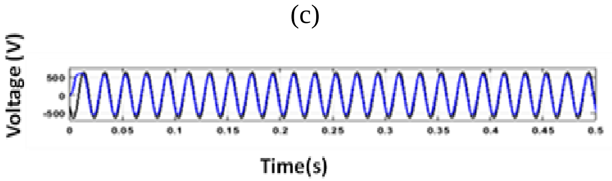

(d)

Fig. 10. Three-phase DIM results: a) voltages unbalanced, b) Output of DIM red phase, c) Output DIM light blue phase, and d) Output of DIM blue phase.

The Three-phase sinusoidal reference signal for the MMC converter is shown in Figure 12(a). Whereas, Inverter output voltage and currents synchronized at t=0.005s are also shown in Figure 12 b.

FFT analysis is performed on the output DIM signal in Figure 13. THD of the DIM signal is less than 0.09%.

A comparative analysis is performed with other Grid synchronization techniques as given in Table 1. The proposed method performs well during dynamic conditions in grid synchronization of the MMC Inverter.

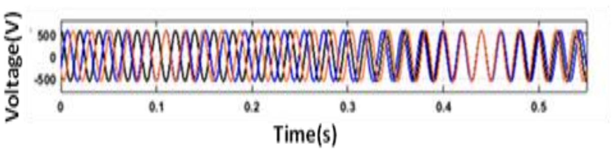

(a)

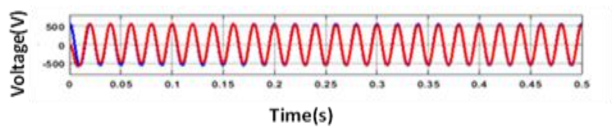

(b)

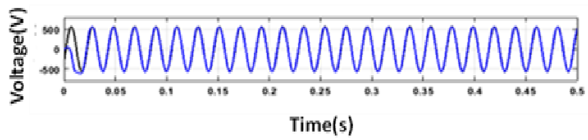

(c)

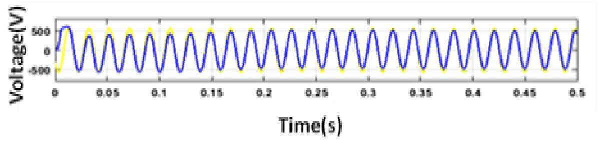

(d)

Fig. 11. Three-phase DIM results: a) frequency unbalanced, b) Output of DIM red phase, c) Output of DIM light blue phase, and d) Output of DIM blue phase.

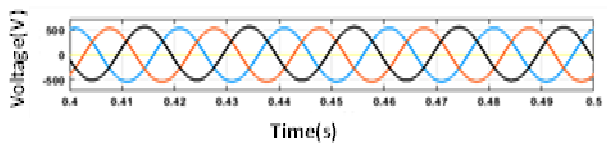

(a)

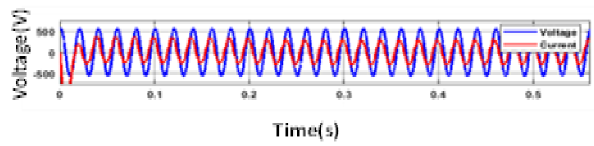

(b)

Fig. 12. a)Three-phase reference signal, and b) Inverter Output voltage and current.

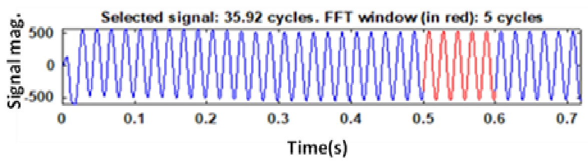

(a)

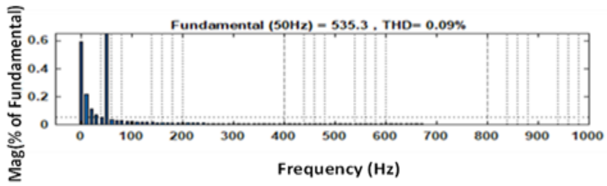

(b)

Fig. 12. FFT analysis: a) Output DIM signal, and b) THD

Table 1. Comparative analysis

Ref.	PLL	Double integration method	DC-Offset rejection	Grid synchronization	Grid Dynamic Conditions	Findings
M. Jabbar Mnati et.al [28]	-	✔	✔	✔	-	Steady state conditions only
Lou et.al [13]	✔	-	✔	✔	-	Time delay caused by filter
S. Golestan et.al [41].	✔	-	✔	✔	-	Loop filtering is not good for dynamic conditions
M. Karimi et.al [21].	✔	-	✔	✔	-	Bandpass filter introduces a phase shift
M. Quraan [42]	✔	-	✔	✔	-	Phase comparator is good during dynamic conditions
Proposed	-	✔	✔	✔	✔	MMC, dynamic conditions

The modelling results show that the output voltage of DIM and the three-phase grid are synchronized and DC offset rejection is also good as compared to other techniques given in Table 1. The DC-offset is as evidenced by the simulation results in Table 2, the use of nonlinear feedback was avoided.

Table 2. Simulation Results

Grid Frequency	Black Phase	Light Blue Phase	Blue Phase
50 Hz	0.005s	0.005s	0.005s

The Three-phase MMC parameters are given in Table 3. The MMC is connected to an AC grid with a voltage rating of 420/380 kV.

Table 3. MMC Parameters for Three-Phase

Parameters	Symbol	Value
Grid side AC voltage	$V_{g(abc)}$	420 kV
Converter side AC voltage	$V_{c(abc)}$	380kV
Transformer connection	T_1/T_2	Y/Δ
Arm capacitor	C	28 µF
Arm inductance	L_{arm}	76 mH
Arm resistance	R	0.8 Ω
Filter inductance	L_1	15mH
Filter resistance	R_1	0.8 Ω
Angular frequency	ω_o	314 rad/s

5. Conclusion

This research paper has proposed Grid synchronization in a Three-phase MMC grid connected Inverter using a Three-phase double integration method. The simulation results demonstrated the efficacy of a three-phase double integration approach in quick grid synchronization at t=0.005s and lower THD levels. In addition to linear delayed feedback, a circuit was developed that eliminates DC offset at each integrator as well as phase error reduction. The results also demonstrated the Three-phase DIM's capacity to synchronize and recover in a grid-connected inverter under non-ideal grid circumstances. The proposed method will be tested with other grid synchronization techniques in the next paper.

References

[1] G.P. Adam, S.J. Finney, K.H. Ahmed and B.W. Williams, "Modular multilevel converter modelling for power system studies,'' 4th International Conference on Power Engineering, Energy and Electrical Drives Istanbul, Turkey, 13-17 May 2013.

[2] M. A. Perez, S. Bernet, J. Rodriguez, S. Kouro, and R. Lizana, "Circuit Topologies, Modeling, Control Schemes, and Applications of Modular Multilevel Converters", in IEEE Transactions on Power Electronics, 2015, vol. 30, no. 1, pp. 4-17

[3] L. D. Zhang, L. Harnefors, H. P. Nee, "Power-Synchronization Control of Grid-Connected Voltage-Source Converters", IEEE Trans. on Power Systems,2010,25(2), pp. 809-820.

[4] P. Rodríguez, A. Luna, R. S. M. Aguilar, I. E.Otadui, R. Teodorescu, F. Blaabjerg "A stationary reference frame grid synchronization system for three-phase grid-connected power converters under adverse grid conditions", IEEE Trans. Power Electron., 2012, 27, (1), pp. 99–112.

[5] A. Ameli, S Bahrami. F.Khazaeli, M. Haghifam, "A Multiobjective Particle Swarm Optimization for Sizing and Placement of DGs from DG Owner's and Distribution Company's Viewpoints", IEEE Trans. Power Deliv. 2014, 29, 1831–1840.

[6] O. Vainio, S. J. Ovaska, "Noise reduction in zero crossing detection by predictive digital filtering", IEEE Trans Ind Electron 1995;42(1):58–62.

[7] L. Lai, W. Chan, "Real-time frequency and harmonic evaluation using artificial neural networks", IEEE Trans Power Deliv 1999;14(1):52–9.

[8] D. Yazdani, A. Bakhshai, G. Joos, M. Mojiri, "A nonlinear adaptive synchronization technique for grid-connected distributed energy sources", IEEE Trans Power Electron 2008;23(4):2181–6.

[9] P. Rodriguez, R. Teodorescu, I. Candela, A. Timbus, M. Liserre, F. Blaabjerg, "New positive-sequence voltage detector for grid synchronization of power converters under faulty grid conditions", In Proceedings of the 2006 37th IEEE Power Electronics Specialists Conference, Jeju, Korea, 18–22 June 2006; pp. 1–7.

[10] Y. Cao, J. Yu, Y. Xu, Y. Li, J. Yu, "An efficient phase-locked loop for distorted three-phase systems", Energies 2017, 10, 280.

[11] N. Hui, D. Wang, Y. Li, "An efficient hybrid filter-based phase-locked loop under adverse grid conditions", Energies 2018, 11, 703.

[12] O. Carranza, E. Figueres, G. Garcerá, L. G. Gonzalez, "Comparative study of speed estimators with highly noisy measurement signals for wind energy generation systems", Appl Energy 2011;88(3):805–13.

[13] W. Luo, J. Jiang, H. Liu, "Frequency-adaptive modified comb-filter-based phase-locked loop for a doubly-fed adjustable-speed pumped-storage hydropower plant under distorted grid conditions", Energies 2017, 10, 737.

[14] F. M. Wulfran, D. N. S. Raoul, M. J. Jacques, and K. T. Saatong, "A technical analysis of a grid-connected hybrid renewable energy system under meteorological constraints for a timely energy management", IJSG, DOI: https://doi. org/10.20508/ijsmartgrid. v7i2, 278, p.g260.

[15] M. Yousefzadeh, H. R. Najafi, and H. Eliasi, "State-space modeling and small-signal stability analysis of an independent microgrid with multiple distributed generation resources", International Journal of Smart Grid-ijSmartGrid, 8(1), pp.1-11.

[16] A. Hooshyar and M. S. Pasand, "Accurate measurement of fault currents contaminated with decaying DC offset and CT saturation", IEEE Trans. Power Del, 2012 vol. 27, no. 2, pp. 773–783.

[17] G. Buticchi, E. Lorenzani, and G. Franceschini, "A dc offset current compensation strategy in transformer less grid-connected power converters", IEEE Trans. Power Del.,2011 vol. 26, no. 4, pp. 2743–2751.

[18] R. Takahashi, K. Abe, H. Takami and F. Ishibashi, "A Proposal of Optimal Current Control for Three-Phase Grid-Connected Inverter with LCL-Filter via IRM-ILQ Method", 2024 13th International Conference on Renewable Energy Research and Applications (ICRERA), Nagasaki, Japan, 2024, pp. 369-374, doi: 10.1109/ICRERA62673.2024.10815263.

[19] A. Bouhouta, S. Moulahoum, N. Kabache, A. Moualdia and I. Colak, "Harmonics compensation of grid-connected PV systems using a novel M5P model tree control", 2023 11th International Conference on Smart Grid (icSmartGrid), Paris, France, 2023, pp. 1-6, doi: 10.1109/icSmartGrid58556.2023.10170901.

[20] M. K. Ghartemani, M. Mojiri, A. Safaee, J. A. Walseth, S. A. Khajehoddin, P. Jain, and A. Bakhshai, "A new phase-locked loop system for three-phase applications", IEEE Trans. Power Electron.,2013 vol. 28, no. 3, pp. 1208–1218.

[21] M. Karimi Ghartemani, S. Khajehoddin, P. Jain, A. Bakhshai, and M. Mojiri, "Addressing DC component in PLL and notch filter algorithms", IEEE Trans. Power Electron.,2012 vol. 27, no. 1, pp. 78–86.

[22] M. Ciobotaru, R. Teodorescu, V. G. Agelidis, "Offset rejection for PLL based synchronization in grid-connected converters", In: Proc 23rd Ann IEEE appl power elect conf and expo (APEC); 2008. p. 1611–7.

[23] S. Golestan, M. Monfared, F. Freijedo, "Design-oriented study of advanced synchronous reference frame phase-locked loops", IEEE Trans Power Electron 2013;28(2):765–78.

[24] H. Shams, J. Yu, and A. W. Shamas, "Modeling and simulation of PV system with three phase inverter along PV, IV curves using MATLAB/Simulink" International Journal of Smart Grid-ijSmartGrid, 7(4), pp.208-217.

[25] A. Yuksel and N. Altin, "Three-phase grid-connected five-level packed U-Cell (PUC-5) inverter design", 2022 11th International Conference on Renewable Energy Research and Application (ICRERA), Istanbul, Turkey, 2022, pp. 490-495, doi: 10.1109/ICRERA55966.2022.9922807.

[26] K. Kusaka and S. Shimura, "Unbalanced Three-phase Flying-capacitor Converter for Current Ripple Reduction", 2024 13th International Conference on Renewable Energy Research and Applications (ICRERA), Nagasaki, Japan, 2024, pp. 1627-1632, doi: 10.1109/ICRERA62673.2024.10815248.

[27] J. M. V. Bikorimana, M. J. Mnati, A. Van den Bossche, "Frequency synchronization of a single-phase grid-connected DC/AC inverter using a double integration method," Automatika, 2017 ,58:2, 141-146.

[28] M. J. Mnati, D. V. Bozalakov, and A. V. Bossche, "A New Synchronization Technique of a Three-Phase Grid Tied Inverter for Photovoltaic Applications", Mathematical Problems in Engineering, vol. 2018, pp-1-18.

[29] J. Hu and H. Ma, "Synchronization of the carrier wave of parallel three-phase inverters with virtual oscillator control", IEEE Transactions on Power Electronics,2017 vol. 32, no. 10, pp. 7998– 8007.

[30] M. Hagiwara, H. Akagi, "PWM control and experiment of modular multilevel converters", In Proceedings of the IEEE Power Electronics Specialists Conference, Rhodes, Greece, 15–19 June 2008; pp. 154–161.

[31] S. Debnath, J. Qin, B. Bahrani, M. Saeedifard, and P. Barbosa, "Operation, control, and applications of the modular multilevel converter: A review", in IEEE Transactions on Power Electronics,2015 vol. 30, no. 1, pp. 37-53.

[32] H. Dommel, "Digital computer solution of electromagnetic transients in single-and multiphase networks", IEEE Trans. Power Appar. Syst. 1969, PAS-88, 388–399.

[33] CIGRE, WG B4-57 Guide for the Development of Models for HVDC Converters in a HVDC Grid; Tech. Broch: Pairs, France, 2014.

[34] N. Ahmed, L. Angquist, S. Norrga, A. Antonopoulos, L. Harnefors, H. P. Nee, "A Computationally efficient continuous model for the modular multilevel converter", IEEE J. Em. Sel. Top. Power Electron. 2014, 2, 1139–1148.

[35] K. D. Hurst, T. G. Habetler, G. Griva, and F. Profumo, "Zero-speed tacholess IM torque control: Simply a matter of stator voltage integration", IEEE Trans. Ind. Applicat., 1998 vol. 34, pp. 790–795.

[36] M. Zerbo, P. Sicard, and A. Ba-Razzouk, "Accurate adaptive integration algorithms for induction machine drive over a wide speed range", in P roceedings of the IEEE International Conference on Electric Machines and Drives (IEMDC), San Antonio, TX, USA, May 15-18 2005, pp. 1082-1088.

[37] F. Wu and X. Li, "Multiple DSC filter-based three-phase EPLL for nonideal grid synchronization", IEEE J. Emerg. Sel. Top. Power Electron. 2017, Vol. 5 (3),pp. 1396–1403.

[38] X. Liu, L. Xiong, B. Wu, Y. Qian, and Y. Liu, "Phase locked-loop with decaying DC transient removal for three-phase grids" Int. J. Electr. Power & Energy Syst. 2022avol.143, pp-108508.

[39] D. Siemaszko, A. Antonopoulos, K. Ilves, M. Vasiladiotis, L. Ängquist, H. Nee, "Evaluation of control and modulation methods for modular multilevel converters", International Power Electronics Conference 2010 746–753.

[40] Q. Tu, Z. Xu, and L. Xu, "Reduced switching-frequency modulation and circulating current suppression for modular multilevel converters", IEEE Trans. Power Del., 2011vol. 26, no. 3, pp. 2009–2017.

[41] S. Golestan, F. D. Freijedo, A. Vidal, A. G. Yepes, J. M. Guerreroand, J. D. Gandoy, "An efficient implementation of generalized delayed signal cancellation PLL", in IEE Transactions on Power Electronics, vol. 31, no. 2, pp. 1085-1094, Feb. 2016.

[42] M. Quraan, "Error compensation algorithm for SRF-PLL in three-phase grid-connected converters", in IEEE Access, vol. 8, pp. 182338-182346, 2020.